Article

Utility of the DHFR-based destabilizing domain across mouse models of retinal degeneration and aging

E. coli DHFR destabilizing domain (DD) system

Use in aged mice (up to 24 mo)

Use in environmentally-induced models of retinal degeneration

(LIRD: light-induced retinal degeneration)

Use in genetic retinal degeneration models

Hui Peng, Prerana Ramadurgum, DaNae R. Woodard, ..., Bo Chen, Rafael Ufret-Vincenty, John D. Hulleman

john.hulleman@utsouthwestern.edu

Highlights

Destabilizing domains (DDs) confer conditional control of ocular protein abundance

The DHFR DD is effectively turned over and stabilized in aged mouse's retina

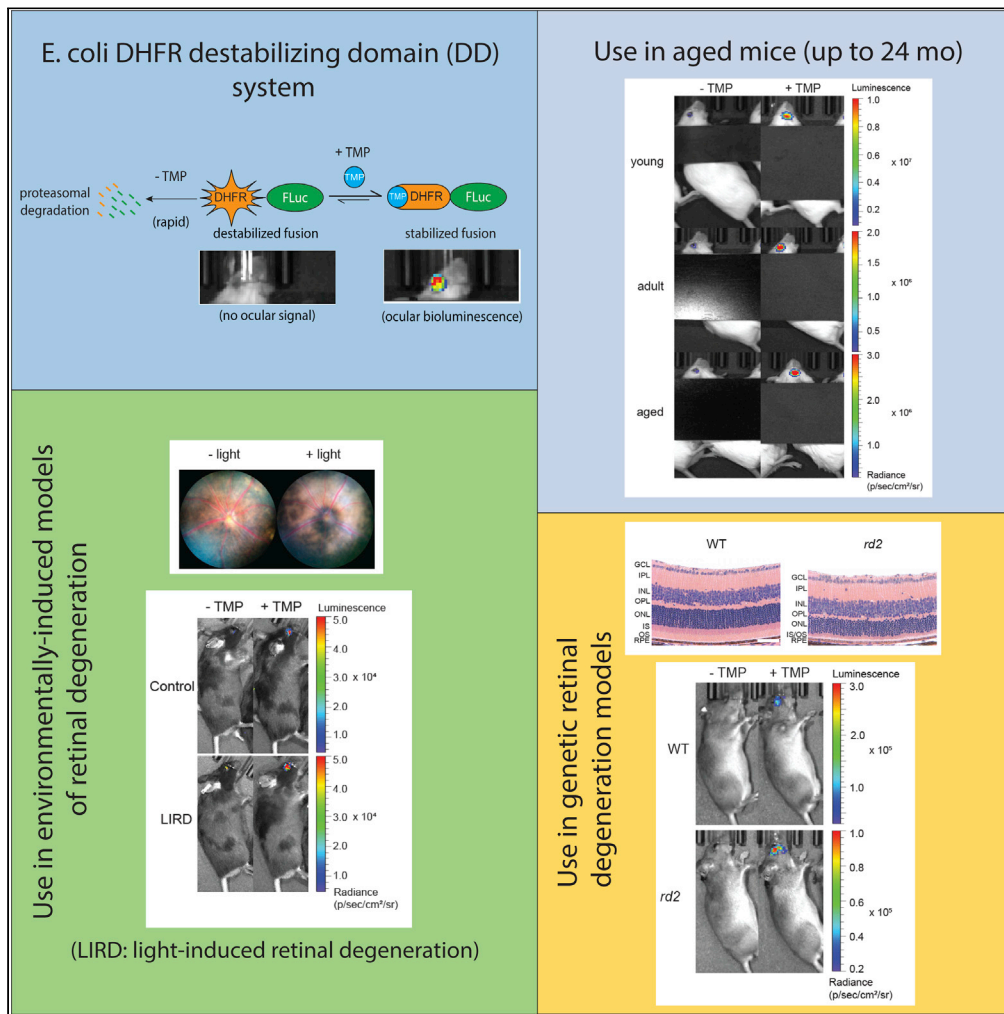DHFR DDs perform well in environmental and genetic retinal degenerative models

Article

Utility of the DHFR-based destabilizing domain across mouse models of retinal degeneration and aging

Hui Peng,[1,3] Prerana Ramadurgum,[1,3] DaNae R. Woodard,[1,3] Steffi Daniel,[1] Emi Nakahara,[1] Marian Renwick,[1] Bogale Aredo,[1] Shyamtanu Datta,[1] Bo Chen,[1] Rafael Ufret-Vincenty,[1] and John D. Hulleman[1,2,4,*]

SUMMARY

The *Escherichia coli* dihydrofolate reductase (DHFR) destabilizing domain (DD) serves as a promising approach to conditionally regulate protein abundance in a variety of tissues. To test whether this approach could be effectively applied to a wide variety of aged and disease-related ocular mouse models, we evaluated the DHFR DD system in the eyes of aged mice (up to 24 months), a light-induced retinal degeneration (LIRD) model, and two genetic models of retinal degeneration (*rd2* and *Abca4*$^{-/-}$ mice). The DHFR DD was effectively degraded in all model systems, including *rd2* mice, which showed significant defects in chymotrypsin proteasomal activity. Moreover, trimethoprim (TMP) administration stabilized the DHFR DD in all mouse models. Thus, the DHFR DD-based approach allows for control of protein abundance in a variety of mouse models, laying the foundation to use this strategy for the conditional control of gene therapies to potentially treat multiple eye diseases.

INTRODUCTION

The number of gene therapy-based approaches for the treatment of eye diseases has increased substantially over the last decade (Garafalo et al., 2020). These efforts have been driven in part because of two phenomena: i) the eye is an alluring target organ for gene therapy because of its ease of accessibility and immune-privilege (Niederkorn and Stein-Streilein, 2010), and ii) the FDA approval of a gene replacement therapy for the treatment of Leber's congenital amaurosis 2 by using recombinant adeno-associated virus (rAAV) to drive expression of the wild-type (WT) *RPE65* gene in retinal pigment epithelium (RPE) cells (Acland et al., 2001). In this particular instance, constant expression of a WT copy of the *RPE65* gene is appropriate for preventing further retinal degeneration because of loss-of-function *RPE65* mutations. However, a controllable or conditional gene therapy approach may be more desirable in certain instances, such as gain-of-function diseases or in scenarios where constitutive expression of a gene of interest may cause phenotoxicity (High and Roncarolo, 2019).

Conventional inducible gene regulation methods, such as tetracycline/doxycycline-based transactivation systems (i.e., Tet-On (Gossen et al., 1995) and Tet-Off (Gossen and Bujard, 1992)), require an extended time frame to activate and reverse because of additional processing time of transcription and translation to reach expected protein levels and prolonged deposition of the regulating molecule (Au - Gomez-Martinez et al., 2013; Das et al., 2016; Sun et al., 2007). In contrast to transcriptionally regulated conditional systems, protein-based regulation approaches such as the *Escherichia coli* dihydrofolate reductase (DHFR) destabilized domain (DD) system (Iwamoto et al., 2010) can directly and conditionally regulate abundance at the protein level after addition of trimethoprim (TMP) (Iwamoto et al., 2010; Sellmyer et al., 2012; Vu et al., 2017) or a TMP-like molecule (Peng et al., 2019; Ramadurgum et al., 2020a, 2020b). Such a system is especially useful when expressed transgenes are potentially toxic if expressed for prolonged periods of time, or when spatiotemporal regulation is required, such as in the case of particular stress-responsive signaling pathways which typically occur in a sinusoidal-like manner (Datta et al., 2019).

The effectiveness of the regulation of the DHFR DD system relies on two primary processes: i) degradation of the DHFR DD fusion protein mediated through the ubiquitin proteasome system (UPS) in the absence of a stabilizer (thus determining the degree of basal expression), and ii) stabilization of the DHFR DD by TMP

[1]Department of Ophthalmology, University of Texas Southwestern Medical Center, 5323 Harry Hines Blvd, Dallas, TX 75390, USA

[2]Department of Pharmacology, University of Texas Southwestern Medical Center, 5323 Harry Hines Blvd, Dallas, TX 75390, USA

[3]These authors contributed equally

[4]Lead contact

*Correspondence: john.hulleman@utsouthwestern.edu

https://doi.org/10.1016/j.isci.2022.104206

or TMP analogs to increase protein abundance (Banaszynski et al., 2006; Chen et al., 2014; Cooley et al., 2014; Maji et al., 2017; Moore et al., 2016; Shoulders et al., 2013; Vu et al., 2017) (this determines the fold induction). Given TMP's broad ability to distribute across bodily tissues (Reeves and Wilkinson, 1979; Sellmyer et al., 2017), combined with its nanomolar AC_{50} in stabilizing the DHFR-DD (Ramadurgum et al., 2020b), the latter phenomena (*in vivo* stabilization by TMP) is typically not a concern. However, previous reports have indicated that aging (Bulteau et al., 2002; Hwang et al., 2007; Kapphahn et al., 2007; Saez and Vilchez, 2014) and retinal degeneration (Ando et al., 2014; Liu et al., 2014; Lobanova et al., 2013; Louie et al., 2002; Shang and Taylor, 2012; Whitcomb et al., 2013) may correlate with compromised targeting of substrates to the proteasome or compromised proteasome activity itself, which, if true, could lead to higher levels of basal expression of the DHFR DD and potentially compromise the researchers' ability to achieve a proper fold induction after stabilizer addition.

Previously, we demonstrated that the DHFR DD system can regulate the expression of yellow fluorescent protein or firefly luciferase as a proof of concept in the retina of young and healthy mice, where the proteasome presumably functions efficiently (Datta et al., 2018; Peng et al., 2019; Ramadurgum et al., 2020b). Yet, an open question is whether this same system is equally effective at regulating protein abundance in aged mice and mice undergoing active retinal degeneration, which are arguably more relevant physiologic contexts for this approach. Therefore, in this study, we evaluated how well the DHFR DD system functioned in the retinas of aged (up to 24 mo) Balb/c and C57BL6/J mice and in a variety of retinal degeneration contexts, both environmental (light-induced retinal degeneration) and genetic (*rd2*, *Abca4*$^{-/-}$) models. Although these latter models are indeed loss-of-function diseases that would benefit from gene replacement therapy, in this work, we have used these systems as a degenerative background to test the functionality of the DHFR DD approach. We found that the DHFR DD system can be used effectively in mice of all ages and models tested, establishing a strong foundation for using the DHFR DD in the eyes of a wide spectrum of healthy and diseased rodent models.

RESULTS

The DHFR DD is turned over efficiently and stabilized effectively in the retina of aged mice

Age is the primary risk factor for the development of age-related macular degeneration (AMD), the leading cause of blindness in the elderly populace in industrialized nations (Wong et al., 2014). Accordingly, certain aged animal models can be utilized to study the potential underpinnings of AMD(Hulleman, 2016) and other age-associated diseases (Ackert-Bicknell et al., 2015; Fletcher et al., 2014). Aging is typically associated with a decrease in protein quality control (Higuchi-Sanabria et al., 2018) and a concomitant increase in cellular dysfunction/stress (Lavretsky and Newhouse, 2012). Although previous studies have indicated that proteasome activity decreases with age in a number of tissues (Bulteau et al., 2002; Hwang et al., 2007; Saez and Vilchez, 2014), human AMD donor eyes demonstrated increased chymotrypsin-specific proteasome activity in the retina with disease progression (Ethen et al., 2007). Thus, it is still unclear whether proteasome activity changes in the retina of aged vs. young subjects. Accordingly, we assessed proteasomal activity and the DHFR DD system in the retina of young (2 months), adult (12 months), and aged (17–24 mo) Balb/c mice (Figure 1). Using fluorescent 7-amino-4-methylcoumarin (AMC)-conjugated polypeptides as substrates (Kisselev and Goldberg, 2005), we measured three proteolytic activities of the proteasome (i.e., chymotrypsin, trypsin, and caspase). Surprisingly, all three proteolytic activities were unchanged in posterior eyecups of mice, regardless of age (Figure 1A). Moreover, we confirmed that the route by which the DHFR DD was degraded intracellularly was via the proteasome (Figures S1A–S1E).

Next, we evaluated if the DHFR DD could function as effectively in aged mouse retinas compared to young mouse retinas in promoting protein degradation in the absence of the stabilizer, TMP. rAAV2/2[MAX], a serotype which transduces the entire neural retina after intravitreal injection (Datta et al., 2018; Reid et al., 2017) encoding for DHFR DD firefly luciferase (DHFR.FLuc), was intravitreally injected into young, adult, and aged Balb/c mice. Based on the observed proteasome activities (Figure 1A), we hypothesized that DHFR.FLuc should be turned-over efficiently across all ages, yielding a similar basal bioluminescent signal in the absence of TMP. Indeed, similar baseline signals were observed in all age groups before TMP administration ("- TMP", Figures 1B and 1C). Moreover, TMP effectively stabilized DHFR.FLuc throughout all ages of mice ("+ TMP") (Figures 1B, 1D, and 1E). Interestingly, the aged mice demonstrated a significantly higher fold induction (15.8 ± 0.6-fold) in bioluminescence after TMP administration when compared to young mice (9.5 ± 0.5-fold, Figure 1E, p ≤ 0.01, unpaired, 2-tailed *t*-test).
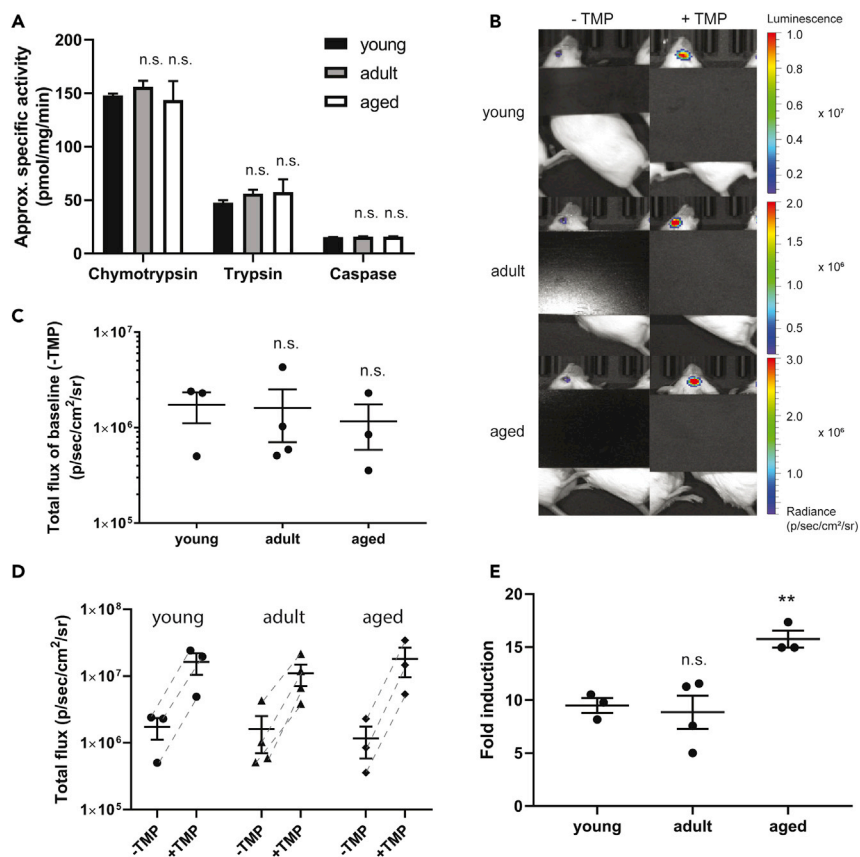
Figure 1. The DHFR DD is turned over efficiently and stabilized effectively in the retina of aged Balb/c mice

(A) Bar chart showing the three specific proteolytic activities (chymotrypsin, trypsin, and caspase activity) in the posterior eyecup of Balb/c mice at 2 months (young), 12 months (adult), and 17–24 months (aged). Data are presented as mean $\pm$ standard deviation (SD) of n = 3.

(B) Representative images of bioluminescence signals originating from intravitreally injected mice at the indicated ages before ("- TMP") and 6 h after TMP treatment (1 mg/mouse via gavage, "+ TMP". n = 3 or 4 mice per age group).

(C) Quantitation of the basal bioluminescence signal in the eye before TMP treatment.

(D) Total flux numbers of the mice plotted before and after TMP treatment.

(E) Fold induction of the bioluminescent signal of each mouse is plotted. For panels (C-E), data are represented as mean $\pm$ SEM. Statistical analysis in panels (A), (C), and (E) was conducted by unpaired, 2-tailed t-test assuming equal variance compared to 2 month 'young' samples, n.s., not significant, **$p < 0.01$. Note: a black tarp is used in (B) to block apparent background luminescence that can originate from the ear tag of the mice.

We paralleled our Balb/c aged mouse experiments in a separate genetic background, the C57BL6/J pigmented mouse. In an assay designed to complement the proteasome activity assay (e.g., Figure 1A), we initially assessed levels of polyubiquitin as well as rhodopsin (ubiquitin-dependent degradation (Saliba et al., 2002)) in adult (8–12 mo) and aged mice (18–22 mo, Figure 2A). We found no demonstrable difference in any of these client proteins (Figure 2A, bands quantified in Figure S2A), suggesting intact and functional degradation capabilities in these mice, reinforcing our observations in aged Balb/c mice. Next, adult and aged mice were intravitreally injected as described previously and tested for baseline and induced DHFR.FLuc bioluminescence. In this pigmented background, the total flux (i.e., bioluminescence) is ∼2 orders of magnitude lower than that observed in nonpigmented mice because of absorbance of the luminescence by pigment. Nonetheless, as observed with Balb/c mice, similar baseline signals were recorded in adult mice compared to aged mice (Figures 2B and 2C). TMP administration promoted DHFR.FLuc stabilization in both ages of mice (Figure 2D); however, as we observed with Balb/c mice (Figure 1E), a significant increase in TMP-mediated fold induction was measured in aged mice (9.3 $\pm$ 0.6-fold) vs. adult mice (5.9 $\pm$ 0.9-fold, Figure 2E, p ≤ 0.01, unpaired, 2-tailed t-test). Although largely speculative, possible explanations for this observed increase could be because of age-related differences in TMP accessibility to the retina owing to blood–retinal barrier breakdown with age (Chan-Ling et al., 2007) or altered TMP pharmacokinetics in older subjects (Siber et al., 1982).
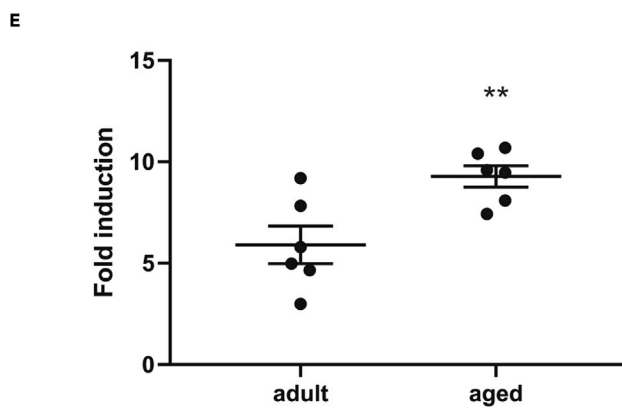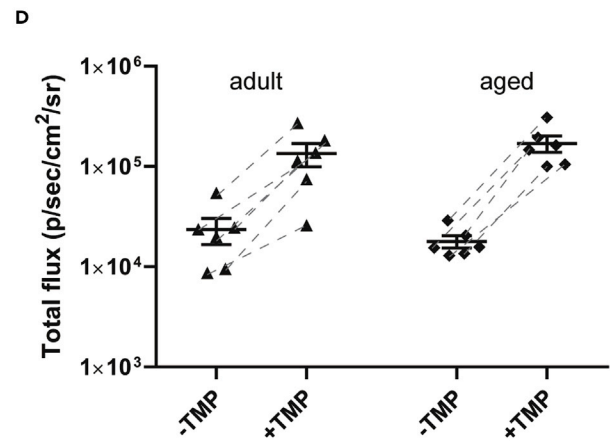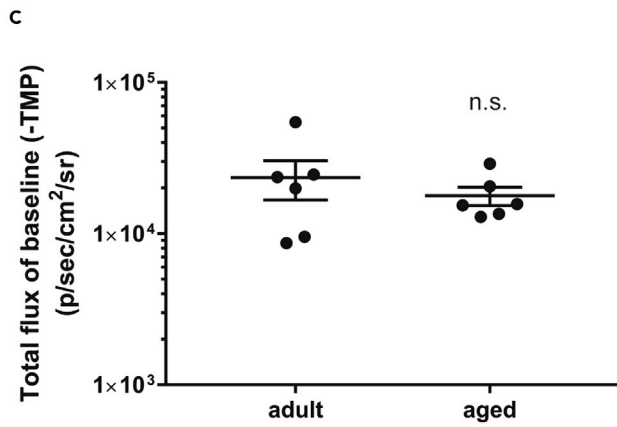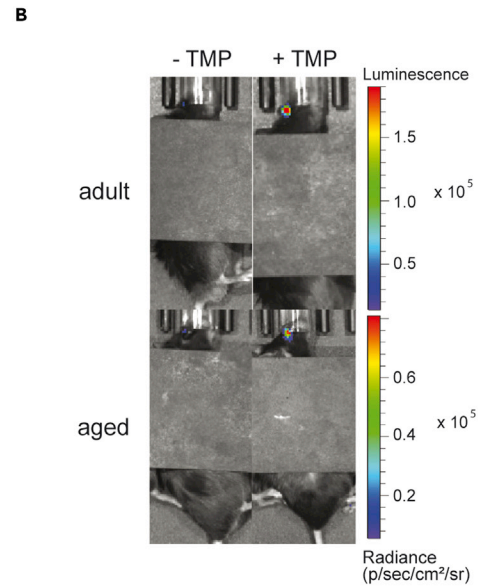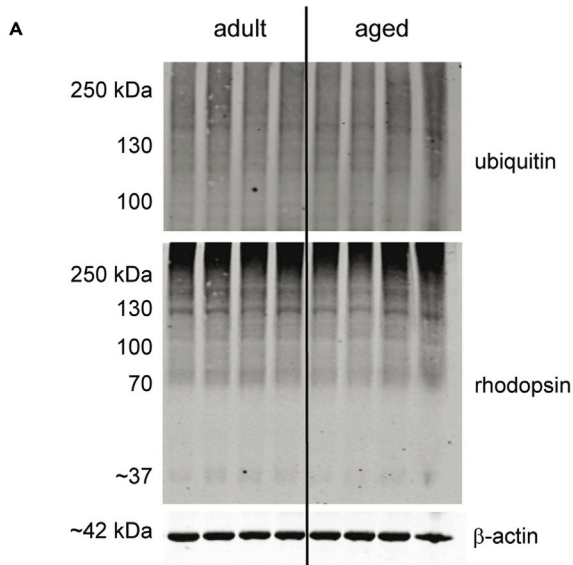
Figure 2. The DHFR DD is degraded efficiently and stabilized readily in the retina of aged C57BL6/J mice

(A) Western blot of adult (12 mo) and aged (20 mo) C57BL6/J mice posterior eyecups using ubiquitin, rhodopsin, and β-actin antibodies (n = 4).

(B) Representative bioluminescent images of intravitreally injected, untreated ("- TMP"), and treated ("+ TMP", 1 mg/mouse, imaged 6 h post gavage, n = 6 mice per age group).

(C) Quantitation of the basal bioluminescence signal in the eye before TMP treatment.

(D) Total flux numbers of the mice plotted before and after TMP treatment.

(E) Fold induction of the bioluminescent signal of each mouse is plotted. For panels (C-E), data are represented as mean ± SEM. Statistical analysis in panels (C) and (E) was conducted by unpaired, 2-tailed t-test assuming equal variance, n.s., not significant, ** p < 0.01. Note: a black tarp is used in (B) to block apparent background luminescence that can originate from the ear tag of the mice.

These DD-based bioluminescence findings in adult and aged mice were additionally verified in separate experiments employing DHFR DD fused to yellow fluorescent protein (DHFR.YFP, Figures S3A–S3D). Moreover, we verified that the observed increase in bioluminescent FLuc signal did not originate from changes in FLuc mRNA transcript levels after TMP stabilization but rather from stabilization at the protein level (Figure S4). Overall, the combination of these bioluminescent and western blotting data demonstrate that multiple DHFR DDs can be efficiently degraded in the absence of TMP while stabilizable in the presence of TMP, regardless of mouse age.

The DHFR DD is degraded and stabilized effectively in the retina of a light-induced retinal degeneration mouse model

Environmental factors, including smoking, diet, and possibly sunlight exposure, have been shown to contribute to the risk and progression of retinal diseases such as AMD, likely by increasing oxidative stress (Ersoy et al., 2014; Wang et al., 2016). Light-induced retinal degeneration (LIRD) is a rapid and aggressive method to induce retinal degeneration (Wenzel et al., 2005) partly through the generation of oxidative stress (Nakanishi et al., 2013), photoreceptor apoptosis (Belmonte et al., 2006), and/or inflammation in the retina (Hadziahmetovic et al., 2012). We induced retinal degeneration using the LIRD method described previously (Zhong et al., 2016) by intraperitoneal injection of fluorescein and subsequent exposure to 50,000 lux of light for 3 min. Fundus images were obtained before ("- light") and 2 days after model generation ("+ light"), showing severe pigmentary changes in a circular area that corresponds to the light exposure area around the optic nerve head after damage (Figure 3A), indicating retinal degeneration (previously verified in more detail) (Zhong et al., 2016). We next measured the proteasome activity in LIRD mice 1 week after light injury and in age-matched, young untreated control mice. Although enhanced apoptosis and the expression of oxidative stress response genes are involved in the LIRD mouse model (Zhong et al., 2016), individual proteasome enzyme activities were not significantly different between LIRD mice and control mice (Figure 3B). Furthermore, probing of select substrates (polyubiquitination, rhodopsin) using western blotting corroborated the proteasome activity findings, demonstrating no appreciable differences between control and LIRD mice (Figure 3C, and quantified in Figure S2B).

Given these promising results, we next evaluated whether mice undergoing LIRD were also able to effectively control DHFR DD abundance as well as control mice. We intravitreally injected C57BL/6J mice AAV encoding for DHFR.FLuc and facilitated AAV expression in the eye for 10 days before LIRD as described previously. Both sets of mice demonstrated a similar ability to degrade the DHFR DD (Figures 3D and 3E). Moreover, there were no significant differences in TMP-induced bioluminescence signals (Figures 3D, 3F, and 3G); control mice showed an 11.7 ± 2.1-fold induction, whereas LIRD mice displayed a 8.3 ± 1.0-fold (Figure 2G), revealing that the DHFR DD was degraded and stabilized effectively in mice actively undergoing LIRD.

The DHFR DD is readily degraded and effectively stabilized in the retina of genetic-retinal degeneration mouse models

A number of naturally occurring and genetically-engineered mouse strains serve as surrogates of human diseases such as retinitis pigmentosa (e.g., the *rd2* mouse, a surrogate for human peripherin mutations that cause retinitis pigmentosa (Chang et al., 2002; Gruning et al., 1994; Keen and Inglehearn, 1996)) and Stargardt disease (e.g., the *Abca4*$^{-/-}$ mouse as a Stargardt disease model (Charbel Issa et al., 2015)). Consequently, these models have been useful in studying disease mechanisms and therapy development. Accordingly, we tested the regulation of the DHFR DD system in these genetic-retinal degeneration mouse models in the hope of eventually applying this conditional gene regulation approach for the treatment of retinal disease.
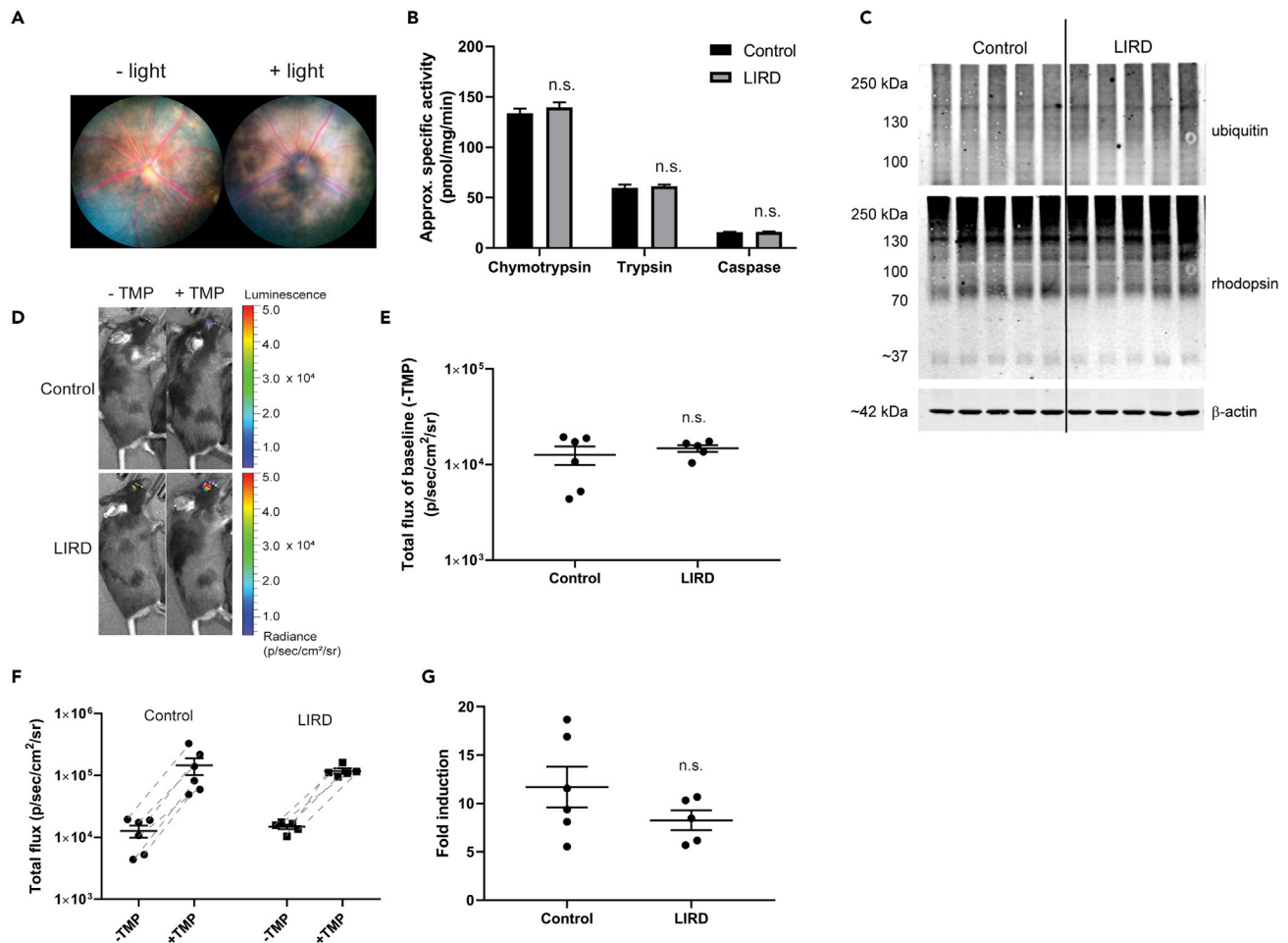
Figure 3. Light-induced retinal degeneration (LIRD) mice maintain the ability to degrade and stabilize the DHFR DD

(A) A representative fundus image before ("- light") and after ("+ light") LIRD (n ≥ 5).

(B) Proteasome enzyme activities in the posterior eyecups of age-matched WT C57BL6/J mice ("control") and LIRD mice harvested 1 week after light injury. Data are represented as mean ± SD, n = 3.

(C) Western blot of control and LIRD mouse posterior eyecups using ubiquitin, rhodopsin, and β-actin antibodies (n = 5).
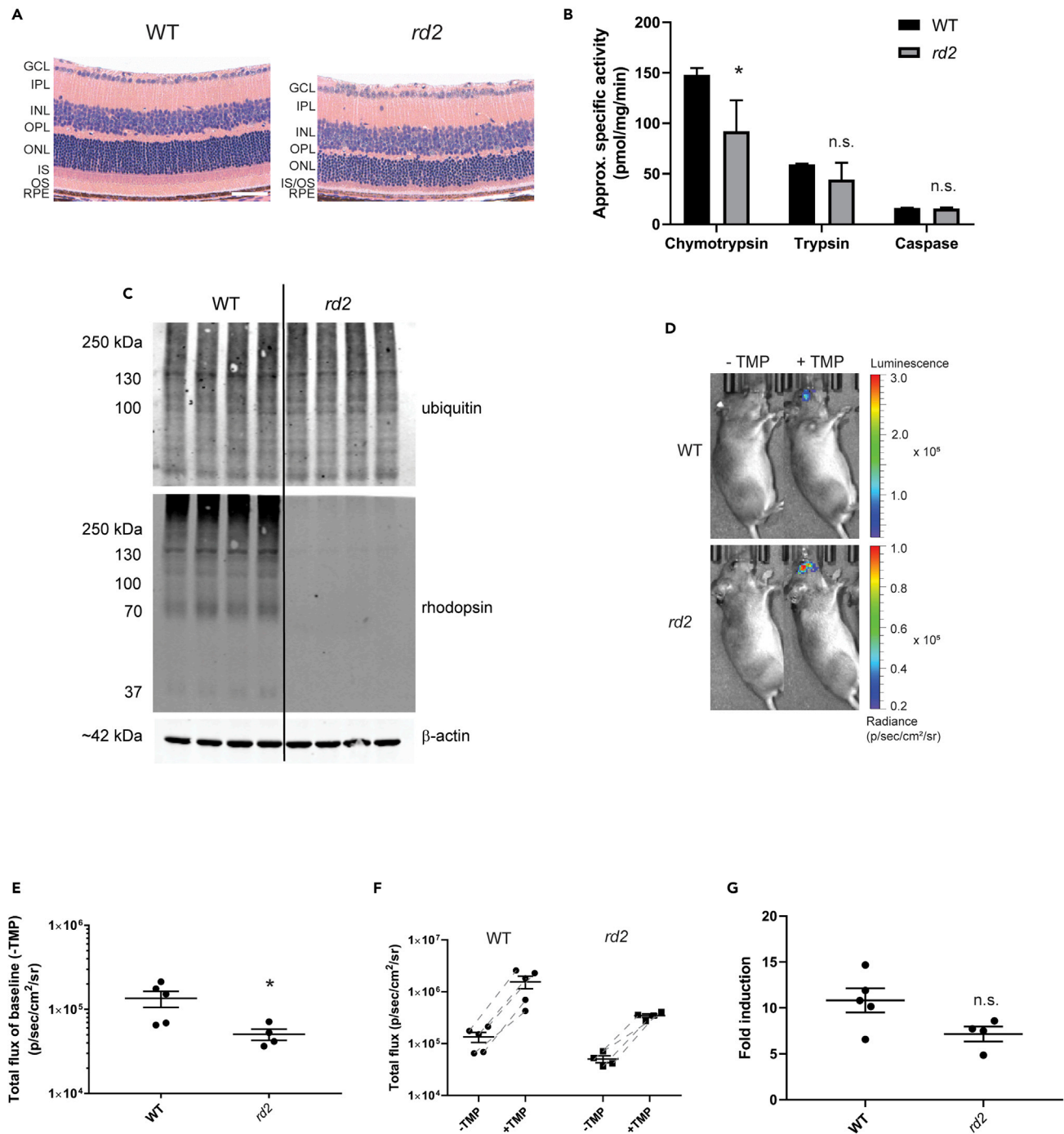
(D) Bioluminescence imaging of representative control and LIRD mice before ("- TMP") and 6 h after TMP treatment (1 mg/mouse via gavage, "+ TMP", n ≥ 5).

(E) Quantitation of basal bioluminescence signal before TMP treatment in control and LIRD mice.

(F) Total flux numbers of control mice and LIRD mice before and after TMP treatment.

(G) The fold induction of the signal of each mouse. Data are represented as mean ± SEM in panels (E-G). Statistical analysis in panels (B), (E), (F), and (G) was conducted by unpaired, 2-tailed t-test assuming equal variance compared to control mice. n.s., not significant.

Rd2 mice lack the Rds/peripherin gene, which encodes a glycoprotein that is required for the formation of photoreceptor outer segment discs (Chang et al., 2002; Kedzierski et al., 2001; Sarra et al., 2001). Homozygous *rd2* mice show an early onset of photoreceptor degeneration, which we confirmed by histology, indicating the loss of outer segment formation by 1 month of age (Figure 4A). Homozygous *rd2* mice demonstrated significantly reduced levels of chymotrypsin (∼40%, Figure 4B, p ≤ 0.05, unpaired, 2-tailed t-test), the predominant enzyme activity of the proteasome. Moreover, when we examined the steady state levels of particular protein substrates by western blot, we detected a virtual absence of rhodopsin (bands quantified in Figure S2C, p < 0.001, unpaired, 2-tailed t-test), presumably because of photoreceptor degeneration, hinting at a robust level of degradative capacity still present (Figure 4C). To examine if the reduced level of proteasome activity was still sufficient to degrade the DHFR DD, we compared the baseline bioluminescence signal generated from subretinal injection of DHFR.FLuc rAAV2/2[MAX] before TMP stabilization. Surprisingly, we found that the basal signal, which implies how readily the DHFR DD is turned over, was significantly lower in *rd2* mice than controls (Figures 4D and

A

WT   *rd2*

GCL
IPL
INL
OPL
ONL
IS
OS
RPE

GCL
IPL
INL
OPL
ONL
IS/OS
RPE

B

WT
rd2

Approx. specific activity (pmol/mg/min)

200
150
100
50
0

Chymotrypsin   Trypsin   Caspase

*   n.s.   n.s.

C

WT   *rd2*

250 kDa
130
100

ubiquitin

250 kDa
130
100
70

37

rhodopsin

~42 kDa

β-actin

D

- TMP   + TMP   Luminescence

WT

3.0
2.0
1.0
x 10⁵

rd2

1.0
0.8
0.6
0.4
0.2
x 10⁵

Radiance
(p/sec/cm²/sr)

E

Total flux of baseline (-TMP) (p/sec/cm²/sr)

1×10⁶
1×10⁵
1×10⁴

WT   *rd2*

*

F

Total flux (p/sec/cm²/sr)

WT   *rd2*

1×10⁷
1×10⁶
1×10⁵
1×10⁴

-TMP +TMP   -TMP +TMP

G

Fold induction

20
15
10
5
0

WT   *rd2*

n.s.

Figure 4. The DHFR DD is readily degraded and effectively stabilized in retinitis pigmentosa model mice

(A) H&E staining showing the retinal cell layers of 1 month WT agouti and homozygous *rd2* mice. RPE: retinal pigment epithelium, OS: outer segment; IS: inner segment; ONL: outer nuclear layer; OPL: outer plexiform layer; INL: inner nuclear layer; IPL: inner plexiform layer, GCL: ganglion cell layer. Scale bar = 50 μm.
(B) Posterior eyecup proteasome enzyme activities of 3 month WT and *rd2* mice, presented as mean ± SD of n = 3.
(C) Western blot of 1 month WT and *rd2* mouse posterior eyecups using ubiquitin, rhodopsin, and β-actin antibodies (n = 4).
(D) Representative bioluminescence images from subretinally injected mice at 1 month before ("- TMP") and after ("+ TMP") TMP treatment, n ≥ 4.
(E) The total flux of basal signal before TMP treatment.
(F) Total flux of the ocular bioluminescent signal was quantified and plotted.
(G) Quantitation of bioluminescence imaging represented as fold induction. In panels (E-G), data are represented as mean ± SEM. Statistics in panels (B), (E), and (G) is analyzed by unpaired, 2-tailed *t*-test assuming equal variance, * $p < 0.05$, n.s., not significant.
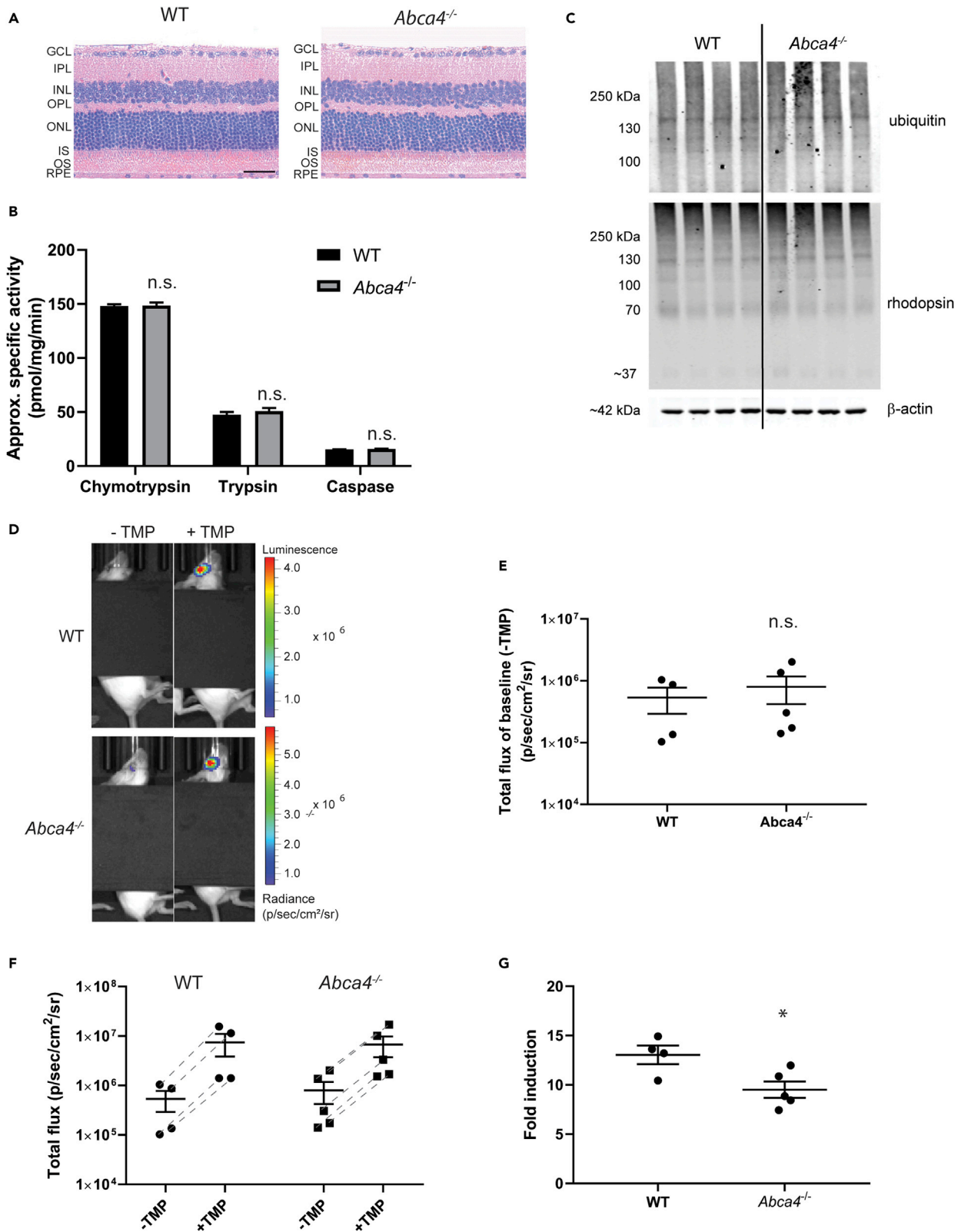
Figure 5. The DHFR DD can be effectively used in a mouse model of Stargardt disease

(A) H&E staining showing the retinal cell layers of 2 month WT and $Abca4^{-/-}$ mice. RPE: retinal pigment epithelium, OS: outer segment; IS: inner segment; ONL: outer nuclear layer; OPL: outer plexiform layer; INL: inner nuclear layer; IPL: inner plexiform layer, GCL: ganglion cell layer. Scale bar = 50 μm.

(B) The three specific proteasome activities were measured in the posterior eyecups of age-matched WT and $Abca4^{-/-}$ 2 month mice. Data are represented as mean ± SD of n = 3. Note: Some WT mice in this panel are the same as the "young" mice in Figure 1A.

(C) Western blot of 6 month-old WT and Abca4$^{-/-}$ posterior eyecups using ubiquitin, rhodopsin, and β-actin antibodies, n = 4.

(D) Representative ocular bioluminescence signals before and after TMP treatment.

(E–G) Quantitation of bioluminescence imaging plotted as basal signal (E), total flux values of control or $Abca4^{-/-}$ mice plotted before ("- TMP") and after TMP ("+ TMP", F), or fold induction of bioluminescent signal of each mouse (G). Data in panels (E-G) are presented as mean ± SEM. Statistical analysis was conducted by unpaired, 2-tailed t-test assuming equal variance compared to WT mice, * p < 0.05, n.s., not significant. Note: a black tarp is used in (D) to block apparent background luminescence that can originate from the ear tag of the mice.

4E), which is the opposite of what we would have predicted based on the chymotrypsin findings (Figure 4B). This is possibly because of loss of photoreceptors that are expressing the DHFR DD during degeneration. Nonetheless, both WT agouti and *rd2* mice produced more bioluminescent signal after TMP treatment (Figures 4D and 4F); the fold induction of bioluminescent signal was lower in the *rd2* mice (7.1 ± 0.8-fold [*rd2*] vs. 10.8 ± 1.5-fold [WT]) but did not reach statistical significance (Figure 4G), suggesting the TMP-induced stabilization of the DHFR DD system in the two mouse groups is similar.

In addition to the *rd2* mice, we also evaluated the induction of DHFR.FLuc in the $Abca4^{-/-}$ mouse, a model of autosomal recessive Stargardt disease (Allikmets et al., 1997; Koenekoop, 2003; Martinez-Mir et al., 1998). These mice lack the Abca4 phospholipid ATPase transporter (located in the photoreceptors and RPE) and are characterized by a progressive increase in bisretinoid autofluorescence and accompanying oxidative, inflammatory, and complement-related stress (Lenis et al., 2017; Radu et al., 2011, 2014) but do not typically show overt histological disruptions of the retina, even by 6 months of age (Figure 5A). As we have performed with the three previous model systems, proteasome activities and select protein clients were measured in WT Balb/c and $Abca4^{-/-}$ mice as described previously (Figures 5B and 5C), with no appreciable differences (Figure S2D). In a separate cohort of rAAV2/2[MAX]-intravitreally-injected mice (injected at ~2 months and allowed to age until 6 months before imaging), the basal bioluminescence signal was quantified in $Abca4^{-/-}$ mice and age-matched WT Balb/c mice (Figures 5D and 5E). Although there is a significant increase in the A500 nm A2E precursor and A2E in $Abca4^{-/-}$ mice at this time point (Radu et al., 2011), which is corroborated by autofluorescent retinal-pigmented epithelium (RPE) flat mounts (Figure S6), the extent of retinal degeneration is not substantial at this age (Charbel Issa et al., 2013) (Figure 5A). Therefore, it was not particularly surprising to observe similar basal bioluminescent signals (Figure 5E) and that TMP could stabilize DHFR.FLuc well in both mouse lines. However, when quantified as fold change in bioluminescent signal, the $Abca4^{-/-}$ mice actually showed a significantly decreased induction (13.1 ± 0.9-fold [WT] vs. 9.5 ± 0.8-fold [Abca4$^{-/-}$], Figure 5G, p ≤ 0.05, unpaired, 2-tailed t-test). Such a minor difference (~27%) would not prevent the application of the DHFR DD system to this mouse model but should be a consideration going forward. Nonetheless, the culmination of these observations validates and extends the use of the DHFR DD system in a range of distinct mouse models of retinal degeneration.

DISCUSSION

Until now, a thorough characterization of the regulation of the DHFR DD strategy for regulating protein abundance in the retina was only tested in young, healthy mice (Datta et al., 2018). In this study, we extended these observations to nonpigmented and pigmented aged mice as well as a series of environmental/genetic retinal degeneration mouse models. We found that for the most part, proteasome activity is largely maintained across these model systems; however, in certain forms of aggressive retinal degeneration, such as the homozygous *rd2* mouse, proteasome activity may be compromised. Similar findings of proteasome overload in various forms of retinal degeneration have also been observed (*rd2* [a.k.a., Rds], and retinitis pigmentosa caused by the P32H mutation in rhodopsin) (Lobanova et al., 2013, 2018). Nonetheless, even with lower proteasome enzyme activity levels observed in *rd2* mice, we never observed higher basal levels of DHFR.FLuc bioluminescence under any conditions, suggesting that there is a fair degree of leeway in retinal proteolytic capacity that affords efficient degradation of the DHFR DD.

The DHFR DD system appears to be increasingly flexible with respect to diversity of model systems to which it can be applied (e.g., yeast (Rakhit et al., 2011), mice, drosophila (Kogenaru and Isalan, 2018), *C. elegans* (Cho et al., 2013)), the proteins it can effectively regulate (Chen et al., 2020; Quintino et al., 2013, 2018; Tai

et al., 2012; Vu et al., 2017), and at the level of the small molecule pharmacological chaperone (Peng et al., 2019; Ramadurgum et al., 2020a, 2020b; Ramadurgum and Hulleman, 2020). With this increasing flexibility comes the ability to apply and fine-tune the DHFR DD system to achieve higher degrees of spatial (guided by AAV or virus tropism and/or a cell-type-specific promoter) and temporal (timing of small molecule administration and/or pharmacokinetic properties) control over protein abundance, and therefore cellular signaling—an exciting prospect for customizable or personalized gene therapy approaches.

In summary, our work demonstrates the efficacy of the DHFR-based system for conditional regulation of protein abundance in aged mice and representative retinal degeneration mouse models, laying the foundation for the application of the DHFR DD system as a biological probe or gene therapy strategy for a variety of distinct mouse models of eye disease.

Limitations of the study

One important limitation of this study is that we were only able to explore a handful of representative retinal degeneration mouse models, which do not cover the entire pathological spectrum of potentially confounding factors. Moreover, except for the aged mice, we evaluated mice at a single time point during the retinal degeneration, which does not account for additional physiological changes that may occur as the disease starts to progress. Future longitudinal studies could shine light onto the long-term stability and biological tolerance for the DHFR DD, although a recent study analyzed mice subretinally injected with an AAV encoding for a mini DHFR degron without any apparent detriment out to 1 year of age (Tornabene et al., 2021). In addition, a more thorough examination of whether particular retinal cell types are recalcitrant to DHFR DD regulatability or whether signal from readily transduced/numerous cells masks the signals from less abundant/less transduced cell types are important aspects to consider. Similarly, inclusion of an additional, constitutively expressed reporter gene in the DHFR DD AAV can help address transduction and regulatability concerns especially under conditions wherein transduced cells may be diseased or eventually die (such as in the *rd2* mouse we used herein). Finally, quantitation of retinal TMP levels and dynamics across model systems could be a variable that factors into the amplitude and duration of DHFR DD stabilization. These future studies will give a more complete picture of the nuances of applying this conditional regulation strategy.

STAR★METHODS

Detailed methods are provided in the online version of this paper and include the following:

- KEY RESOURCES TABLE
- RESOURCE AVAILABILITY
  - Lead contact
  - Materials availability
  - Data and code availability
- EXPERIMENTAL MODEL AND SUBJECT DETAILS
  - Animals
  - Cell lines
- METHOD DETAILS
  - Proteasome activity assay
  - Intravitreal injections
  - Subretinal injections
  - Bioluminescence imaging
  - OCT embedding and cryosectioning and staining
  - Western blotting
  - Fundus camera-delivered light-induced retinal degeneration (FCD-LIRD) mouse model generation
  - Hematoxylin and eosin (H&E) staining
  - Evaluation of DHFR DD mode of degradation
- QUANTIFICATION AND STATISTICAL ANALYSIS

SUPPLEMENTAL INFORMATION

Supplemental information can be found online at https://doi.org/10.1016/j.isci.2022.104206.

ACKNOWLEDGMENTS

AUTHOR CONTRIBUTIONS

Conceptualization, J.D.H.; Methodology, R.U.V. and J.D.H.; Investigation, H.P., P.R., D.R.W., S.D., E.N., M.R., B.A., S.D., and B.C.; Writing – Original Draft, H.P. and J.D.H.; Writing – Review & Editing, H.P., P.R., D.R.W., S.D., E.N., M.R., B.A., S.D., B.C., R.U.V., and J.D.H.; Funding Acquisition, J.D.H.; Supervision, R.U.V. and J.D.H.

DECLARATION OF INTERESTS

The authors declare no competing interests.

INCLUSION AND DIVERSITY

We worked to ensure sex balance in the selection of non-human subjects. One or more of the authors of this paper self-identifies as an underrepresented ethnic minority in science. One or more of the authors of this paper received support from a program designed to increase minority representation in science.

REFERENCES

Ackert-Bicknell, C.L., Anderson, L.C., Sheehan, S., Hill, W.G., Chang, B., Churchill, G.A., Chesler, E.J., Korstanje, R., and Peters, L.L. (2015). Aging Research using mouse models. Curr. Protoc. Mouse Biol. 5, 95–133. https://doi.org/10.1002/9780470942390.mo140195.

Acland, G.M., Aguirre, G.D., Ray, J., Zhang, Q., Aleman, T.S., Cideciyan, A.V., Pearce-Kelling, S.E., Anand, V., Zeng, Y., Maguire, A.M., et al. (2001). Gene therapy restores vision in a canine model of childhood blindness. Nat. Genet. 28, 92–95. https://doi.org/10.1038/88327.

Allikmets, R., Singh, N., Sun, H., Shroyer, N.F., Hutchinson, A., Chidambaram, A., Gerrard, B., Baird, L., Stauffer, D., Peiffer, A., et al. (1997). A photoreceptor cell-specific ATP-binding transporter gene (ABCR) is mutated in recessive Stargardt macular dystrophy. Nat. Genet. 15, 236–246. https://doi.org/10.1038/ng0397-236.

Ando, R., Noda, K., Tomaru, U., Kamoshita, M., Ozawa, Y., Notomi, S., Hisatomi, T., Noda, M., Kanda, A., Ishibashi, T., et al. (2014). Decreased proteasomal activity causes photoreceptor degeneration in MiceAn animal model of senescence acceleration. Invest. Ophthalmol. Vis. Sci. 55, 4682–4690. https://doi.org/10.1167/iovs.13-13272.

Au - Gomez-Martinez, M., Au - Schmitz, D., and Au - Hergovich, A. (2013). Generation of stable human cell lines with tetracycline-inducible (Tet-on) shRNA or cDNA expression. JoVE 5, e50171. https://doi.org/10.3791/50171.

Banaszynski, L.A., Chen, L.-c., Maynard-Smith, L.A., Ooi, A.G.L., and Wandless, T.J. (2006). A rapid, reversible, and tunable method to regulate protein function in living cells using synthetic small molecules. Cell 126, 995–1004. https://doi.org/10.1016/j.cell.2006.07.025.

Belmonte, M.A., Santos, M.F., Kihara, A.H., Yan, C.Y.I., and Hamassaki, D.E. (2006). Light-induced photoreceptor degeneration in the mouse involves activation of the small GTPase Rac1. Invest. Ophthalmol. Vis. Sci. 47, 1193–1200. https://doi.org/10.1167/iovs.05-0446.

Bulteau, A.L., Szweda, L.I., and Friguet, B. (2002). Age-dependent declines in proteasome activity in the heart. Arch. Biochem. Biophys. 397, 298–304. https://doi.org/10.1006/abbi.2001.2663.

Chan-Ling, T., Hughes, S., Baxter, L., Rosinova, E., McGregor, I., Morcos, Y., van Nieuwenhuyzen, P., and Hu, P. (2007). Inflammation and breakdown of the blood-retinal barrier during "physiological aging" in the rat retina: a model for CNS aging. Microcirculation 14, 63–76. https://doi.org/10.1080/10739680601073451.

Chang, B., Hawes, N.L., Hurd, R.E., Davisson, M.T., Nusinowitz, S., and Heckenlively, J.R. (2002). Retinal degeneration mutants in the mouse. Vis. Res. 42, 517–525. https://doi.org/10.1016/S0042-6989(01)00146-8.

Charbel Issa, P., Barnard, A.R., Herrmann, P., Washington, I., and MacLaren, R.E. (2015). Rescue of the Stargardt phenotype in Abca4 knockout mice through inhibition of vitamin A dimerization. Proc. Natl. Acad. Sci. U S A 112, 8415–8420. https://doi.org/10.1073/pnas.1506960112.

Charbel Issa, P., Barnard, A.R., Singh, M.S., Carter, E., Jiang, Z., Radu, R.A., Schraermeyer, U., and MacLaren, R.E. (2013). Fundus autofluorescence in the Abca4(-/-) mouse model of Stargardt disease–correlation with accumulation of A2E, retinal function, and histology. Invest. Ophthalmol. Vis. Sci. 54, 5602–5612. https://doi.org/10.1167/iovs.13-11688.

Chen, J., Lin, F.L., Leung, J.Y.K., Tu, L., Wang, J.H., Chuang, Y.F., Li, F., Shen, H.H., Dusting, G.J., Wong, V.H.Y., et al. (2020). A drug-tunable Flt23k gene therapy for controlled intervention in retinal neovascularization. Angiogenesis 24, 97–110. https://doi.org/10.1007/s10456-020-09745-7.

Chen, J.J., Genereux, J.C., Qu, S., Hulleman, J.D., Shoulders, M.D., and Wiseman, R.L. (2014). ATF6 activation reduces the secretion and extracellular aggregation of destabilized variants of an amyloidogenic protein. Chem. Biol. 21, 1564–1574. https://doi.org/10.1016/j.chembiol.2014.09.009.

Cho, U., Zimmerman, S.M., Chen, L.C., Owen, E., Kim, J.V., Kim, S.K., and Wandless, T.J. (2013). Rapid and tunable control of protein stability in Caenorhabditis elegans using a small molecule. PLoS One 8, e72393. https://doi.org/10.1371/journal.pone.0072393.

Cooley, C.B., Ryno, L.M., Plate, L., Morgan, G.J., Hulleman, J.D., Kelly, J.W., and Wiseman, R.L. (2014). Unfolded protein response activation reduces secretion and extracellular aggregation of amyloidogenic immunoglobulin light chain. Proc. Natl. Acad. Sci. U S A *111*, 13046–13051. https://doi.org/10.1073/pnas.1406050111.

Das, A.T., Tenenbaum, L., and Berkhout, B. (2016). Tet-on systems for doxycycline-inducible gene expression. Curr. Gene Ther. *16*, 156–167.

Datta, S., Peng, H., and Hulleman, J.D. (2019). Small molecule-based inducible gene therapies for retinal degeneration. Adv. Exp. Med. Biol. *1185*, 65–69. https://doi.org/10.1007/978-3-030-27378-1_11.

Datta, S., Renwick, M., Chau, V.Q., Zhang, F., Nettesheim, E.R., Lipinski, D.M., and Hulleman, J.D. (2018). A destabilizing domain allows for fast, noninvasive, conditional control of protein abundance in the mouse eye - implications for ocular gene therapy. Invest. Ophthalmol. Vis. Sci. *59*, 4909–4920. https://doi.org/10.1167/iovs.18-24987.

Ersoy, L., Ristau, T., Hahn, M., Karlstetter, M., Langmann, T., Dröge, K., Caramoy, A., den Hollander, A.I., and Fauser, S. (2014). Genetic and environmental risk factors for age-related macular degeneration in persons 90 Years and older. Invest. Ophthalmol. Vis. Sci. *55*, 1842–1847. https://doi.org/10.1167/iovs.13-13420.

Ethen, C.M., Hussong, S.A., Reilly, C., Feng, X., Olsen, T.W., and Ferrington, D.A. (2007). Transformation of the proteasome with age-related macular degeneration. FEBS Lett. *581*, 885–890. https://doi.org/10.1016/j.febslet.2007.01.061.

Fletcher, E.L., Jobling, A.I., Greferath, U., Mills, S.A., Waugh, M., Ho, T., de Iongh, R.U., Phipps, J.A., and Vessey, K.A. (2014). Studying age-related macular degeneration using animal models. Optom. Vis. Sci. *91*, 878–886. https://doi.org/10.1097/OPX.0000000000000322.

Garafalo, A.V., Cideciyan, A.V., Heon, E., Sheplock, R., Pearson, A., WeiYang Yu, C., Sumaroka, A., Aguirre, G.D., and Jacobson, S.G. (2020). Progress in treating inherited retinal diseases: early subretinal gene therapy clinical trials and candidates for future initiatives. Prog. Retin. Eye Res. *77*, 100827. https://doi.org/10.1016/j.preteyeres.2019.100827.

Gossen, M., and Bujard, H. (1992). Tight control of gene expression in mammalian cells by tetracycline-responsive promoters. Proc. Natl. Acad. Sci. *89*, 5547.

Gossen, M., Freundlieb, S., Bender, G., Muller, G., Hillen, W., and Bujard, H. (1995). Transcriptional activation by tetracyclines in mammalian cells. Science *268*, 1766.

Gruning, G., Millan, J.M., Meins, M., Beneyto, M., Caballero, M., Apfelstedt-Sylla, E., Bosch, R., Zrenner, E., Prieto, F., and Gal, A. (1994). Mutations in the human peripherin/RDS gene associated with autosomal dominant retinitis pigmentosa. Hum. Mutat. *3*, 321–323. https://doi.org/10.1002/humu.1380030326.

Hadziahmetovic, M., Kumar, U., Song, Y., Grieco, S., Song, D., Li, Y., Tobias, J.W., and Dunaief, J.L. (2012). Microarray analysis of murine retinal light damage reveals changes in iron regulatory, complement, and antioxidant genes in the neurosensory retina and isolated RPE. Invest. Ophthalmol. Vis. Sci. *53*, 5231–5241. https://doi.org/10.1167/iovs.12-10204.

High, K.A., and Roncarolo, M.G. (2019). Gene therapy. N. Engl. J. Med. *381*, 455–464. https://doi.org/10.1056/NEJMra1706910.

Higuchi-Sanabria, R., Frankino, P.A., Paul, J.W., 3rd, Tronnes, S.U., and Dillin, A. (2018). A futile battle? Protein quality control and the stress of aging. Dev. Cell *44*, 139–163. https://doi.org/10.1016/j.devcel.2017.12.020.

Hulleman, J.D. (2016). Malattia leventinese/doyne honeycomb retinal dystrophy: similarities to age-related macular degeneration and potential therapies. Adv. Exp. Med. Biol. *854*, 153–158.

Hwang, J.S., Hwang, J.S., Chang, I., and Kim, S. (2007). Age-associated decrease in proteasome content and activities in human dermal fibroblasts: restoration of normal level of proteasome subunits reduces aging markers in fibroblasts from elderly persons. J. Gerontol. Biol. Sci. Med. Sci. *62*, 490–499. https://doi.org/10.1093/gerona/62.5.490.

Iwamoto, M., Bjorklund, T., Lundberg, C., Kirik, D., and Wandless, T.J. (2010). A general chemical method to regulate protein stability in the mammalian central nervous system. Chem. Biol. *17*, 981–988. https://doi.org/10.1016/j.chembiol.2010.07.009.

Kapphahn, R.J., Bigelow, E.J., and Ferrington, D.A. (2007). Age-dependent inhibition of proteasome chymotrypsin-like activity in the retina. Exp. Eye Res. *84*, 646–654. https://doi.org/10.1016/j.exer.2006.12.002.

Kedzierski, W., Nusinowitz, S., Birch, D., Clarke, G., McInnes, R.R., Bok, D., and Travis, G.H. (2001). Deficiency of rds/peripherin causes photoreceptor death in mouse models of digenic and dominant retinitis pigmentosa. Proc. Natl. Acad. Sci. *98*, 7718. https://doi.org/10.1073/pnas.141124198.

Keen, T.J., and Inglehearn, C.F. (1996). Mutations and polymorphisms in the human peripherin-RDS gene and their involvement in inherited retinal degeneration. Hum. Mutat. *8*, 297–303. https://doi.org/10.1002/(sici)1098-1004(1996)8:4<297::aid-humu1>3.0.co;2-5.

Kisselev, A.F., and Goldberg, A.L. (2005). Monitoring activity and inhibition of 26S proteasomes with fluorogenic peptide substrates. Methods Enzymol. *398*, 364–378. https://doi.org/10.1016/s0076-6879(05)98030-0.

Koenekoop, R.K. (2003). The gene for Stargardt disease, ABCA4, is a major retinal gene: a mini-review. Ophthalmic Genet. *24*, 75–80.

Kogenaru, M., and Isalan, M. (2018). Drug-inducible control of lethality genes: a low background destabilizing domain architecture applied to the Gal4-UAS system in Drosophila. ACS Synth. Biol. *7*, 1496–1506. https://doi.org/10.1021/acssynbio.7b00302.

Lavretsky, H., and Newhouse, P.A. (2012). Stress, inflammation, and aging. Am. J. Geriatr.

Psychiatr. *20*, 729–733. https://doi.org/10.1097/JGP.0b013e31826573cf.

Lenis, T.L., Sarfare, S., Jiang, Z., Lloyd, M.B., Bok, D., and Radu, R.A. (2017). Complement modulation in the retinal pigment epithelium rescues photoreceptor degeneration in a mouse model of Stargardt disease. Proc. Natl. Acad. Sci. U S A *114*, 3987–3992. https://doi.org/10.1073/pnas.1620299114.

Liu, Z., Qin, T., Zhou, J., Taylor, A., Sparrow, J.R., and Shang, F. (2014). Impairment of the ubiquitin-proteasome pathway in RPE alters the expression of inflammation related genes. Adv. Exp. Med. Biol. *801*, 237–250. https://doi.org/10.1007/978-1-4614-3209-8_31.

Lobanova, E.S., Finkelstein, S., Li, J., Travis, A.M., Hao, Y., Klingeborn, M., Skiba, N.P., Deshaies, R.J., and Arshavsky, V.Y. (2018). Increased proteasomal activity supports photoreceptor survival in inherited retinal degeneration. Nat. Commun. *9*, 1738. https://doi.org/10.1038/s41467-018-04117-8.

Lobanova, E.S., Finkelstein, S., Skiba, N.P., and Arshavsky, V.Y. (2013). Proteasome overload is a common stress factor in multiple forms of inherited retinal degeneration. Proc. Natl. Acad. Sci. U S A *110*, 9986–9991. https://doi.org/10.1073/pnas.1305521110.

Louie, J.L., Kapphahn, R.J., and Ferrington, D.A. (2002). Proteasome function and protein oxidation in the aged retina. Exp. Eye Res. *75*, 271–284. https://doi.org/10.1006/exer.2002.2022.

Maji, B., Moore, C.L., Zetsche, B., Volz, S.E., Zhang, F., Shoulders, M.D., and Choudhary, A. (2017). Multidimensional chemical control of CRISPR-Cas9. Nat. Chem. Biol. *13*, 9–11. https://doi.org/10.1038/nchembio.2224.

Martinez-Mir, A., Paloma, E., Allikmets, R., Ayuso, C., del Rio, T., Dean, M., Vilageliu, L., Gonzalez-Duarte, R., and Balcells, S. (1998). Retinitis pigmentosa caused by a homozygous mutation in the Stargardt disease gene ABCR. Nat. Genet. *18*, 11–12. https://doi.org/10.1038/ng0198-11.

Moore, C.L., Dewal, M.B., Nekongo, E.E., Santiago, S., Lu, N.B., Levine, S.S., and Shoulders, M.D. (2016). Transportable, chemical genetic methodology for the small molecule-mediated inhibition of heat shock factor 1. ACS Chem. Biol. *11*, 200–210. https://doi.org/10.1021/acschembio.5b00740.

Nakanishi, T., Shimazawa, M., Sugitani, S., Kudo, T., Imai, S., Inokuchi, Y., Tsuruma, K., and Hara, H. (2013). Role of endoplasmic reticulum stress in light-induced photoreceptor degeneration in mice. J. Neurochem. *125*, 111–124. https://doi.org/10.1111/jnc.12116.

Niederkorn, J.Y., and Stein-Streilein, J. (2010). History and physiology of immune privilege. Ocul. Immunol. Inflamm. *18*, 19–23. https://doi.org/10.3109/09273940903564766.

Peng, H., Chau, V.Q., Phetsang, W., Sebastian, R.M., Stone, M.R.L., Datta, S., Renwick, M., Tamer, Y.T., Toprak, E., Koh, A.Y., et al. (2019). Non-antibiotic small-molecule regulation of DHFR-based destabilizing domains in vivo. Molecular therapy. Methods Clin. Dev. *15*, 27–39. https://doi.org/10.1016/j.omtm.2019.08.002.

Quintino, L., Manfre, G., Wettergren, E.E., Namislo, A., Isaksson, C., and Lundberg, C. (2013). Functional neuroprotection and efficient regulation of GDNF using destabilizing domains in a rodent model of Parkinson's disease. Mol. Ther. 21, 2169–2180. https://doi.org/10.1038/mt.2013.169.

Quintino, L., Namislo, A., Davidsson, M., Breger, L.S., Kavanagh, P., Avallone, M., Elgstrand-Wettergren, E., Isaksson, C., and Lundberg, C. (2018). Destabilizing domains enable long-term and inert regulation of GDNF expression in the brain. Molecular therapy. Methods Clin. Dev. 11, 29–39. https://doi.org/10.1016/j.omtm.2018.08.008.

Radu, R.A., Hu, J., Jiang, Z., and Bok, D. (2014). Bisretinoid-mediated complement activation on retinal pigment epithelial cells is dependent on complement factor H haplotype. J. Biol. Chem. 289, 9113–9120. https://doi.org/10.1074/jbc.M114.548669.

Radu, R.A., Hu, J., Yuan, Q., Welch, D.L., Makshanoff, J., Lloyd, M., McMullen, S., Travis, G.H., and Bok, D. (2011). Complement system dysregulation and inflammation in the retinal pigment epithelium of a mouse model for Stargardt macular degeneration. J. Biol. Chem. 286, 18593–18601. https://doi.org/10.1074/jbc.M110.191866.

Rakhit, R., Edwards, S.R., Iwamoto, M., and Wandless, T.J. (2011). Evaluation of FKBP and DHFR based destabilizing domains in Saccharomyces cerevisiae. Bioorg. Med. Chem. Lett. 21, 4965–4968. https://doi.org/10.1016/j.bmcl.2011.06.006.

Ramadurgum, P., Daniel, S., and Hulleman, J.D. (2020a). Protocol for in vivo evaluation and use of destabilizing domains in the eye, liver, and beyond. STAR Protoc. 1, 100094. https://doi.org/10.1016/j.xpro.2020.100094.

Ramadurgum, P., and Hulleman, J.D. (2020). Protocol for designing small-molecule-regulated destabilizing domains for in vitro use. STAR Protoc. 1, 100069. https://doi.org/10.1016/j.xpro.2020.100069.

Ramadurgum, P., Woodard, D.R., Daniel, S., Peng, H., Mallipeddi, P.L., Niederstrasser, H., Mihelakis, M., Chau, V.Q., Douglas, P.M., Posner, B.A., and Hulleman, J.D. (2020b). Simultaneous control of endogenous and user-defined genetic pathways using unique ecDHFR pharmacological chaperones. Cell Chem. Biol. 27, 622–634.e6. https://doi.org/10.1016/j.chembiol.2020.03.006.

Reeves, D.S., and Wilkinson, P.J. (1979). The pharmacokinetics of trimethoprim and trimethoprim/sulphonamide combinations, including penetration into body tissues. Infection 7 (Suppl 4), S330–S341. https://doi.org/10.1007/BF01639009.

Reid, C.A., Ertel, K.J., and Lipinski, D.M. (2017). Improvement of photoreceptor targeting via intravitreal delivery in mouse and human retina using combinatory rAAV2 capsid mutant VectorsImproved intravitreal AAV delivery to photoreceptors. Invest. Ophthalmol. Vis. Sci. 58,

6429–6439. https://doi.org/10.1167/iovs.17-22281.

Saez, I., and Vilchez, D. (2014). The mechanistic links between proteasome activity, aging and age-related diseases. Curr. Genom. 15, 38–51. https://doi.org/10.2174/1389202915011403061133344.

Sahu, B., Chavali, V.R., Alapati, A., Suk, J., Bartsch, D.U., Jablonski, M.M., and Ayyagari, R. (2015). Presence of rd8 mutation does not alter the ocular phenotype of late-onset retinal degeneration mouse model. Mol. Vis. 21, 273–284.

Saliba, R.S., Munro, P.M.G., Luthert, P.J., and Cheetham, M.E. (2002). The cellular fate of mutant rhodopsin: quality control, degradation and aggresome formation. J. Cell Sci. 115, 2907–2918.

Sarra, G.-M., Stephens, C., de Alwis, M., Bainbridge, J.W.B., Smith, A.J., Thrasher, A.J., and Ali, R.R. (2001). Gene replacement therapy in the retinal degeneration slow (rds) mouse: the effect on retinal degeneration following partial transduction of the retina. Hum. Mol. Genet. 10, 2353–2361. https://doi.org/10.1093/hmg/10.21.2353.

Schalken, J.J., Janssen, J.J., Sanyal, S., Hawkins, R.K., and de Grip, W.J. (1990). Development and degeneration of retina in rds mutant mice: immunoassay of the rod visual pigment rhodopsin. Biochim. Biophys. Acta. 1033, 103–109. https://doi.org/10.1016/0304-4165(90)90201-7.

Sellmyer, M.A., Chen, L.C., Egeler, E.L., Rakhit, R., and Wandless, T.J. (2012). Intracellular context affects levels of a chemically dependent destabilizing domain. PLoS One 7, e43297. https://doi.org/10.1371/journal.pone.0043297.

Sellmyer, M.A., Lee, I., Hou, C., Weng, C.C., Li, S.H., Lieberman, B.P., Zeng, C.B., Mankoff, D.A., and Mach, R.H. (2017). Bacterial infection imaging with [F-18]fluoropropyl-trimethoprim. Proc. Natl. Acad. Sci. U S A 114, 8372–8377. https://doi.org/10.1073/pnas.1703109114.

Shang, F., and Taylor, A. (2012). Chapter 10 - role of the ubiquitin–proteasome in protein quality control and signaling: implication in the pathogenesis of eye diseases. In Progress in Molecular Biology and Translational Science, T. Grune, ed. (Academic Press), pp. 347–396. https://doi.org/10.1016/B978-0-12-397863-9.00010-9.

Shoulders, M.D., Ryno, L.M., Cooley, C.B., Kelly, J.W., and Wiseman, R.L. (2013). Broadly applicable methodology for the rapid and dosable small molecule-mediated regulation of transcription factors in human cells. J. Am. Chem. Soc. 135, 8129–8132. https://doi.org/10.1021/ja402756p.

Siber, G.R., Gorham, C.C., Ericson, J.F., and Smith, A.L. (1982). Pharmacokinetics of intravenous trimethoprim-sulfamethoxazole in children and adults with normal and impaired renal function. Rev. Infect. Dis. 4, 566–578. https://doi.org/10.1093/clinids/4.2.566.

Sun, N., Shibata, B., Hess, J.F., and FitzGerald, P.G. (2015). An alternative means of retaining ocular structure and improving immunoreactivity for light microscopy studies. Mol. Vis. 21, 428–442.

Sun, Y., Chen, X., and Xiao, D. (2007). Tetracycline-inducible expression systems: new strategies and practices in the transgenic mouse modeling. Acta Biochim. Biophys. Sin. 39, 235–246. https://doi.org/10.1111/j.1745-7270.2007.00258.x.

Tai, K., Quintino, L., Isaksson, C., Gussing, F., and Lundberg, C. (2012). Destabilizing domains mediate reversible transgene expression in the brain. PLoS One 7, e46269. https://doi.org/10.1371/journal.pone.0046269.

Tornabene, P., Trapani, I., Centrulo, M., Marrocco, E., Minopoli, R., Lupo, M., Iodice, C., Gesualdo, C., Simonelli, F., Surace, E.M., and Auricchio, A. (2021). Inclusion of a degron reduces levelsof undesired inteins after AAV-mediated proteintrans-splicing in the retina. Molecular therapy. Methods Clin. Dev. 23, 448–459. https://doi.org/10.1016/j.omtm.2021.10.004.

Vu, K.T., Zhang, F., and Hulleman, J.D. (2017). Conditional, genetically encoded, small molecule-regulated inhibition of NFkappaB signaling in RPE cells. Invest. Ophthalmol. Vis. Sci. 58, 4126–4137. https://doi.org/10.1167/iovs.17-22133.

Wang, W., Gawlik, K., Lopez, J., Wen, C., Zhu, J., Wu, F., Shi, W., Scheibler, S., Cai, H., Vairavan, R., et al. (2016). Genetic and environmental factors strongly influence risk, severity and progression of age-related macular degeneration. Signal Transduct. Target. Ther. 1, 16016. https://doi.org/10.1038/sigtrans.2016.16.

Wenzel, A., Grimm, C., Samardzija, M., and Reme, C.E. (2005). Molecular mechanisms of light-induced photoreceptor apoptosis and neuroprotection for retinal degeneration. Prog. Retin. Eye Res. 24, 275–306. https://doi.org/10.1016/j.preteyeres.2004.08.002.

Whitcomb, E.A., Shang, F., and Taylor, A. (2013). Common cell biologic and biochemical changes in aging and age-related diseases of the eye: toward new therapeutic approaches to age-related ocular DiseasesAge-related biochemical changes in the eye. Invest. Ophthalmol. Vis. Sci. 54, ORSF31–ORSF36. https://doi.org/10.1167/iovs.13-12808.

Wong, W.L., Su, X.Y., Li, X., Cheung, C.M.G., Klein, R., Cheng, C.Y., and Wong, T.Y. (2014). Global prevalence of age-related macular degeneration and disease burden projection for 2020 and 2040: a systematic review and meta-analysis. Lancet Glob. Health 2, E106–E116. https://doi.org/10.1016/S2214-109x(13)70145-1.

Zhong, X., Aredo, B., Ding, Y., Zhang, K., Zhao, C.X., and Ufret-Vincenty, R.L. (2016). Fundus camera-delivered light-induced retinal degeneration in mice with the RPE65 Leu450Met variant is associated with oxidative stress and apoptosis. Invest. Ophthalmol. Vis. Sci. 57, 5558–5567. https://doi.org/10.1167/iovs.16-19965.

STAR★METHODS

KEY RESOURCES TABLE

REAGENT or RESOURCE	SOURCE	IDENTIFIER
Antibodies		
rabbit anti-rhodopsin	Cell Signaling Technologies	14825S
mouse anti-ubiquitin	Santa Cruz	sc-8017
mouse anti-HA	Pierce	26183
mouse anti-beta actin	Sigma-Aldrich	A1978
mouse anti-GFP	Invitrogen	A11120
rabbit anti-mCherry	Abcam	ab167453
anti-mouse AlexaFluor488	Invitrogen	A28175
anti-rabbit AlexaFluor594	Invitrogen	A32740
Bacterial and virus strains		
rAAV2/2[MAX] DHFR.YFP 2A mCherry	Hulleman Laboratory	N/A
rAAV2/2[MAX] NanoLuc 2A DHFR.FLuc	Hulleman Laboratory	N/A
Biological samples		
neural retina	various mouse strains	N/A
Chemicals, peptides, and recombinant proteins		
Suc-Leu-Leu-Val-Tyr-AMC	Cayman Chemical	10008119
Boc-Leu-Arg-Arg-AMC	AdipoGen	AG-CP3-0014-M001
Ac-Nle-Pro-Nle-Asp-AMC	Cayman Chemical	21639
MG-132	Cayman Chemical	10012628
cyclopentolate hydrochloride	Alcon	N/A
Tropicamide	Alcon	N/A
GenTeal (severe dry eye)	Alcon	N/A
Hanks buffered salt solution (HBSS)	Sigma-Aldrich	H8264-6X500ML
Tween-20	Fisher Scientific	BP337-500
bacitracin zinc and polymyxin B sulfate ointment	Bausch & Lomb	N/A
Luciferin	GoldBio	LUCK
Trimethoprim	Sigma-Aldrich	T7883-100G
DMSO	Fisher Scientific	BP231-100
Tween-80	Fisher Scientific	BP338-500
Cremaphor	Sigma-Aldrich	238470
PEG400	Fisher Scientific	P167-1
Dextrose	Fisher Scientific	D15-500
Paraformaldehyde	Electron Miscroscopy Sciences	1574
Phosphate buffered saline (PBS)	Fisher Scientific	BP2944100
optimal cutting temperature compound	Tissue-Tek	4583
Triton X-100	Fisher Scientific	BP-151-100
goat serum	Gibco	16210064
ProLong Diamond Antifade with DAPI	Life Technologies	P36961
radioimmunoprecipitation assay (RIPA) buffer	Santa Cruz	sc-24948
Halt Protease Inhibitor Cocktail	Pierce	78430

(Continued on next page)

Continued

REAGENT or RESOURCE	SOURCE	IDENTIFIER
proteasome assay lysis buffer (50 mM Tris HCl, pH 7.5, 40 mM KCl, 5 mM MgCl$_2$, 1 mM DTT and 0.5 mM ATP)	Hulleman Laboratory	N/A
Odyssey Blocking Buffer	LI-COR	927-40000
Tris-Gly SDS PAGE buffer	Hulleman Laboratory	N/A
Ponceau S	Sigma-Aldrich	P7170-1L
Fluorescein	Akorn	N/A
Methanol	Fisher Scientific	A412-4
acetic acid	Fisher Scientific	A38-212
Ethanol	Fisher Scientific	A4094
Isopentane	Fisher Scientific	O3551-4
Chloroquine	MP Biomedicals	0219391910
ketamine/xylazine	UT Southwestern Animal Resource Center	N/A
ammonium chloride	Sigma-Aldrich	A9434
Critical commercial assays		
bicinchoninic acid assay	Pierce	23225
Experimental models: Cell lines		
CHO/dhFr- cells	ATCC	CRL-9096
Experimental models: Organisms/strains		
C3A *Pde6b*[rd1].O20/A-*Prph2*[Rd2]/J (rd2) mice	The Jackson Laboratory	001979
wild-type agouti mice	The Jackson Laboratory	001912
wild-type Balb/c mice	Hulleman Laboratory (from R345W$^{+/-}$ mice breeding schemes)	N/A
Abca4 $^{-/-}$ mice (Balb/c background)	Dr. Roxana Radu	N/A
wild-type C57BL/6J mice	UT Southwestern Breeding Core	N/A
Software and algorithms		
Image Studio	LI-COR	N/A
Excel	Microsoft	N/A
Word	Microsoft	N/A
GraphPad Prism	GraphPad Software	N/A

RESOURCE AVAILABILITY

Lead contact

For additional information and requests for data should be directed to the lead contact Dr. John D. Hulleman, Ph.D (John.Hulleman@utsouthwestern.edu).

Materials availability

Unique reagents (e.g., the NanoLuc 2A DHFR-FLuc construct) are available upon request to the lead author.

Data and code availability

Data reported in this paper will be shared by the lead contact upon request. This paper does not report original code.

EXPERIMENTAL MODEL AND SUBJECT DETAILS

Animals

All animal experiments were performed according to the guidelines of the Association for Research in Vision and Ophthalmology (ARVO) Statement for the Use of Animals in Ophthalmic and Vision Research

and were approved by the Institutional Animal Care and Use Committee (IACUC) of UT Southwestern Medical Center, Dallas, TX, USA. Equal numbers of age-matched, littermate male and female mice were used whenever possible. Mice were provided standard laboratory chow and allowed free access to water, in a climate-controlled room with a 12 h light/12 h dark cycle. WT Balb/c mice originated from heterozygous breeding schemes from R345W$^{+/-}$ EFEMP1 mice (courtesy of Dr. Lihua Marmorstein, private stock at The Jackson Laboratory, Bar Harbor, ME). WT C57BL/6J control and experimental mice used for light-induced retinal degeneration experiments were purchased from the UT Southwestern Mouse Breeding Core and were genotyped to confirm the absence of the potentially confounding rd8 mutation (Sahu et al., 2015). WT adult (8–12 mo), aged (20–22 mo) C57BL6/J mice, rd2 (stock # 001979 (Schalken et al., 1990)), and WT agouti (stock # 001912) mice were also obtained from The Jackson Laboratory. Abca4$^{-/-}$ mice in the Balb/c background (Lenis et al., 2017) were obtained from Dr. Roxana Radu, Jules Stein Eye Institute, University of California Los Angeles.

Cell lines

Female Chinese hamster ovary (CHO) cells (CHO/dhFr-, CRL-9096, ATCC) were used in this study. Standard growth conditions (37°C, 5% CO$_2$) were used for culturing. Low passage cells were used. Short tandem repeat (STR) authentication was not performed since our normal provider for this service (University of Arizona Genomics Core) indicated that their assay could only distinguish human cells.

METHOD DETAILS

Proteasome activity assay

Mice were euthanized by overdose of ketamine/xylazine (180 mg/kg, 24 mg/kg, respectively) and their eyes were enucleated to prepare posterior eyecup samples. The anterior segment of the eye, the optic nerve, and the muscles attached to the outside of the eyeball were discarded, and the remaining posterior eyecups from both eyes were snap-frozen in liquid nitrogen and stored at −80°C until use. When ready to use, the posterior eyecup samples were homogenized on ice in 600 μL lysis buffer containing 50 mM Tris HCl, pH 7.5, 40 mM KCl, 5 mM MgCl$_2$, 1 mM DTT and 0.5 mM ATP. The crude cell lysate was centrifuged at 17,000 g for 20 min at 4°C and the supernatant was collected. Protein concentration in the supernatant was quantified by a bicinchoninic acid (BCA) assay (Piece, Rockford, IL, USA). Note: the small amount of DTT in the lysis buffer does contribute to a minimal amount of BCA signal; therefore, the resulting specific activity of this assay is considered an approximation. Fifty μL of ∼0.25 mg/mL protein was used to measure proteasome activity by using a proteasome activity assay kit (BioVision, Milpitas, CA, USA). All the components in the kit were used except for the provided substrate. Instead of using the provided substrate, separate substrates were purchased and used to evaluate each proteasomal protease activity. Final concentrations of 100 μM Suc-Leu-Leu-Val-Tyr-AMC (Cayman Chemical, Ann Arbor, MI, USA), Boc-Leu-Arg-Arg-AMC (AdipoGen, San Diego, CA, USA) or Ac-Nle-Pro-Nle-Asp-AMC (Cayman Chemical) were used as substrates to measure chymotrypsin-, trypsin- and caspase-specific proteolytic activity, respectively. A 1.5 h kinetics curve was monitored at 37°C using a Synergy 2 multi-mode microplate reader (BioTek, Winooski, VT, USA). The absolute amount of cleaved substrate was calculated by an AMC standard curve. The assay was conducted with and without 100 μM MG-132 (see Figure S7, Sigma-Aldrich, St. Louis, MO, USA) to confirm proteasomal specificity of the AMC generation. All proteasome assay data were performed in parallel across the model systems.

Intravitreal injections

Intravitreal injections were conducted on Balb/c, C57BL6/J, and Abca4$^{-/-}$ mice following the protocol described previously (Datta et al., 2018; Peng et al., 2019). Mice were anesthetized with a ketamine/xylazine cocktail (120 mg/kg, 16 mg/kg, respectively) followed by pupillary dilation using cyclopentolate hydrochloride (1% [w/v]) (Alcon, Fort Worth, TX, USA) and tropicamide (1% [w/v]) (Alcon). GenTeal eye gel (severe dry eye formula, Alcon) was applied before injection to prevent corneal drying. A Stemi 305 stereo microscope (Zeiss, Oberkochen, Germany) was used to assist with the injection. The right eye was pierced by a 30G needle approximately 1 mm posterior to the supratemporal limbus. Then a 33G ½ needle fitted to a Hamilton micro-syringe (Hamilton, Reno, NV, USA) was inserted into the previous incision at a 45-degree angle until needlepoint was mid-vitreous. Two microliters of rAAV2/2[MAX] (Reid et al., 2017) encoding for Nano luciferase 2A DHFR.FLuc (7 × 10^9 viral genomes, prepared by the UNC Viral Vector Core, Chapel Hill, NC, USA) was slowly injected into the vitreous over the course of ∼1 min. Note: Nano luciferase was not used in these studies because of issues with substrate administration and penetrance into the eye. Afterwards, the

needle was held stable for an additional minute before slowly removed. The left eye was injected with a sham vehicle (HBSS with 0.14% Tween [HBSS-T]) using the same injection procedure. After injection, bacitracin zinc and polymyxin B sulfate ointment (Bausch & Lomb, Tampa, FL, USA) and GenTeal eye gel were applied to each eye. Mice were kept warm on a heating pad until regaining consciousness. For Balb/c mice shown in Figure 1, and C57BL6/J mice shown in Figure 2, mice at the indicated ages were injected with AAV ~10 days prior to initial baseline imaging and subsequent imaging post stabilization with TMP. Young LIRD mice were intravitreally injected with AAV 10 days prior to initiation of the LIRD protocol. $Abca4^{-/-}$ mice were injected at ~2 mo with AAV and allowed to age out to 6 mo prior to baseline and stabilization readings.

Subretinal injections

WT agouti and $rd2$ mice at four days postnatal (P4) were anesthetized on ice until they stopped moving. Using a Stemi 305 stereo microscope to assist with the injection, the eyelid was slit by a 25G 5/8 needle to allow the eye to proptose. The right eye was pierced by a 30G needle approximately 1 mm posterior to the supratemporal limbus. Then a 33G ½ needle with blunt tip fitted to a Hamilton micro-syringe was inserted into the previous incision at a 45-degree angle until the needlepoint met resistance posterior to the retina. Half a microliter of rAAV2/2[MAX] encoding for DHFR.FLuc or DHFR.YFP 2A mCherry (1×10^9 viral genomes) was injected into the subretinal space. The left eye was injected with a sham vehicle (HBSS with 0.14% Tween [HBSS-T]) using the same injection procedure. After injection, bacitracin zinc and polymyxin B sulfate ointment was applied to each eye. Mice were kept warm on a heating pad until regaining consciousness. Mice were imaged for baseline bioluminescence and stabilization at 1 mo of age.

Bioluminescence imaging

To establish an initial baseline signal, mice were placed in an IVIS Spectrum *In Vivo* Imaging System (UT Southwestern Small Animal Imaging Resource, PerkinElmer, Waltham, MA, USA) under anesthesia by circulating isoflurane. Each mouse was injected intraperitoneally with 150 mg luciferin/kg body weight, and the eyes were imaged for bioluminescence over a 20-min time course with 1 min interval between every image. At times, a black tarp was used to cover the mice to prevent background signal due to an ear tag. The next day mice were given 1 mg TMP (~50 mg/kg depending on mouse weight). Specifically, TMP was dissolved in 20 μL DMSO and then diluted with 40 μL PEG400 (Fisher Scientific, Waltham, MA, USA), 4 μL Tween 80 (Fisher Scientific), 20 μL cremaphor (Sigma-Aldrich) and 116 μL of 5% dextrose (Fisher Scientific) and administered by oral gavage. Six hours after oral gavage, the mice were imaged again in the same manner as described for basal signal establishment. The total flux number at the peak of the kinetics and the image with the peak number were used for plotting and comparison between "- TMP" and "+ TMP". While in this manuscript we have performed bioluminescence imaging on Balb/c, C57BL6/J and agouti mice, we should note that Balb/c and agouti mice are preferred due to absence or reduction in ocular pigmentation. C57BL6/J can be used, but typically yield much lower absolute basal bioluminescence.

OCT embedding and cryosectioning and staining

Eyes were harvested and fixed in 4% paraformaldehyde for 2 h. Following 3 brief washes in 1× PBS, they were embedded in Tissue-Tek OCT compound, frozen and stored until ready for sectioning. Eyes were sectioned at a thickness of 12 μm using a cryostat and mounted on glass slides. Slides were dried for 30 min at 37°C on a slide warmer. Slides were rehydrated in 1× PBS and pre-treated with 0.1% Triton X-100/1× PBS for 10 min. Sections were then incubated in blocking buffer (10% goat serum [Gibco, #16210064, New Zealand origin] in 0.1% Triton X-100/1× PBS) for 2 h at room temperature (RT) in a dark and humidified chamber. Sections were then incubated overnight with primary antibodies reconstituted in blocking buffer (mouse anti-GFP, 1:500, Invitrogen #A-11120; rabbit anti-mCherry, 1:500, Abcam #ab167453). Following three washes in 1× PBS, sections were incubated with secondary antibodies (anti-mouse AlexaFluor488, 1:1000, Invitrogen #A28175; anti-rabbit AlexaFluor594, 1:1000, Invitrogen #A32740) for 2 h at room temperature. Sections were washed in 1× PBS and mounted with Pro-Long Diamond Antifade medium containing DAPI (Life Technologies #P36961). Images were acquired at × 25 magnification using a Leica TCS SP8 confocal microscope (Leica Microsystems).

Western blotting

For protein analysis involving ubiquitin or rhodopsin, mouse posterior eyecups were lysed with radioimmunoprecipitation assay (RIPA) buffer (Santa Cruz, Dallas, TX, USA) supplemented with Halt protease inhibitor

(Pierce, Rockford, IL, USA) and benzonase (Millipore Sigma, St. Louis, MO, USA) and homogenized on ice using a Bel-Art™ Micro-Tube Homogenizer (Fisher Scientific, Waltham, MA, USA, cat# 03-421-215). For experiments involving assessment of the DHFR.YFP protein, neural retina was peeled from the eye cup and homogenized as described above. After homogenization, samples were incubated on ice for 10 min then spun at max speed (14,800 rpm) at 4°C for 10 min. The supernatant was collected and protein concentration was quantified via a bicinchoninic assay (BCA) assay (Pierce Thermo Scientific, Rockford, IL, USA). Approximately 30 μg of soluble supernatant was run on a 4%–20% Tris-Gly SDS PAGE gel (Life Technologies) and transferred onto a nitrocellulose membrane using an iBlot2 device (Life Technologies). After probing for total protein transferred using Ponceau S (Sigma-Aldrich), membranes were blocked overnight in Odyssey Blocking Buffer (LICOR, Lincoln, NE, USA). Membranes were probed with rabbit anti-rhodopsin (1:1000; Cell Signaling Technologies, Danvers, MA. USA cat# 14825S), mouse anti-ubiquitin (1:1000; Santa Cruz, Dallas, TX. USA, cat# sc-8017), mouse anti-HA (1:1500, Pierce, Waltham, MA, clone 2-2.2.14, cat# 26183), and mouse anti-β-actin (1:5000; Sigma-Aldrich, cat# A1978). All Western blot imaging was performed on an Odyssey CLx (LI-COR) and band quantification was performed using Image Studio software (LI-COR).

Fundus camera-delivered light-induced retinal degeneration (FCD-LIRD) mouse model generation

Ten days after intravitreal AAV injection, a group of randomly picked mice was designated as control (virus injected, fluorescein-injected, no light-induced degeneration) while the rest were used for the severe FCD-LIRD model (Zhong et al., 2016), here after simply referred to as LIRD. An advantage of this specific method is that one can induce retinal damage in the common C57BL6/J background. As previously described (Zhong et al., 2016), LIRD-designated mice were dark adapted overnight, and the next morning anesthetized with a ketamine/xylazine cocktail (120 mg/kg, 16 mg/kg, respectively) followed by pupillary dilation using cyclopentolate hydrochloride (1% [w/v]) and tropicamide (1% [w/v]). GenTeal eye gel was also applied to prevent dry cornea. After a clear fundus image was taken, mice were injected with fluorescein (2 mg, i.p.), incubated for 10 min, and subsequently exposed to 50,000 lux of light for 3 min (continuously). Afterwards, bacitracin zinc and polymyxin B sulfate ointment was applied to the eye, and mice were kept warm on a heating pad until regaining consciousness. Two days after model generation, the fundus images of the LIRD-designated eyes were obtained to confirm retinal degeneration.

Hematoxylin and eosin (H&E) staining

WT agouti mice and *rd2* mice at 1 mo were euthanized by ketamine/xylazine overdose. WT Balb/c and *Abca4*$^{-/-}$ mice at 6 mo were euthanized similarly. Eyes were rapidly enucleated and processed for freeze substitution following previous literature recommendations (Sun et al., 2015) with slight modification. Enucleated eyes were submerged in chilled isopentane for 1 min, transferred to chilled 97% methanol and 3% acetic acid (MAA) and stored at −80°C for 48 h. Then the vial was warmed stepwise to −20°C for 24 h, followed by 4°C for 4 h, and then room temperature for 2 h. MAA was then replaced with 100% ethanol and the eye was processed into paraffin-embedded sections. H&E staining was performed by the UT Southwestern Histo Pathology core and images of the sections were taken at 40 × magnification using an inverted epifluorescent microscope (Zeiss).

Evaluation of DHFR DD mode of degradation

Chinese hamster ovary (CHO) cells (CHO/dhFr-, CRL-9096, ATCC) stably expressing DHFR DD YFP were seeded into 96 well plate at a density of 10,000 cells per well and allowed to attach overnight. Cells were then treated with different concentrations of MG-132 (1 μM), chloroquine (100 μM) or ammonium chloride (50 mM) in quadruplicate and imaged for YFP fluorescence 6 h later on a Celigo Imaging Cytometer (Nexcelom, Lawrence, MA). The assay was performed three independent times.

QUANTIFICATION AND STATISTICAL ANALYSIS

Exact value of n's, what n represents, precision measures, and statistical methods can be found listed within each figure legend.